Session 3P2
Advanced Methods for Light Scattering Analysis in Nanotechnology and Biophotonics

Numerical Comparison of Light Scattering Results by Particles in Free Space Obtained by Discrete Dipole Approximation and Volume Integral Equation Methods

V. I. Ivakhnenko
ADE Corporation, USA

Rigorous numerical methods are applied widely for light scattering modeling by nanoparticles located in different media. The most flexible methods that allow simulate arbitrary shaped particles and to take into account permittivity distribution inside the particle and its anisotropy properties as well are Discrete Dipole Approximation (DDA) [1] and Volume Integral Equation (VIE) [2] methods. Both methods look rather similar: they are based on numerical solution of Electric field integral equation for unknown function inside the volume of scatter; the conditions at infinity are taken into account analytically; fast Fourier transform (FFT) technique is utilized in numerical solution of linear equation system in order to accelerate matrix-vector multiplications. Nevertheless, DDA method allows accurate calculations of electromagnetic scattering from targets with "size parameters" $2\pi a/\lambda < 15$ provided the refractive index m is not large compared to unity ($\mid m-1 \mid < 1$) where as VIE method area of application is significantly wider. This is illustrated at Fig. 1 where the elements of Jone's matrix for the light scattering by spherical particle calculated by DDA and VIE codes are compared to Mie theory. It is important to underline that the same mesh was used in calculations for DDA and VIE methods.

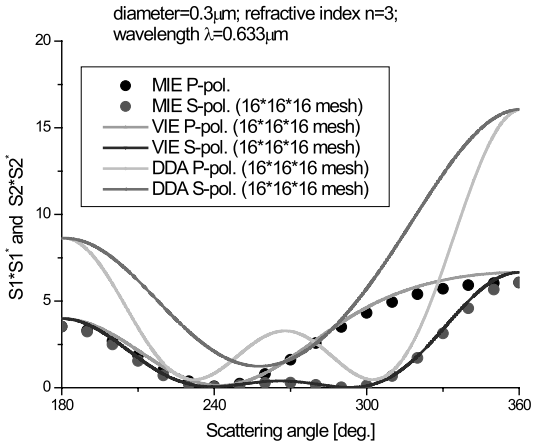

Figure 1.

Analysis of DDA and VIE matrixes structure allows explain why DDA provides rather accurate results for the small values of refractive index but failed for high values.

*Author would like to acknowledge support of this work by ADE Corporation, Westwood, MA, USA.

REFERENCES

1. Draine, B. T. and P. J. Flatau, *J. Opt. Soc. Am. A,* Vol. 11, 1491–1499, 1994.
2. Eremin, Y. and V. Vakhnenko, *JQSRT*, Vol. 60, 475–482, 1998.

Analysis of Evanescent Waves Scattering by a Single Particle in Total Internal Reflection Microscopy

E. Eremina[1], **T. Wriedt**[1], **and L. Helden**[2]
[1]University of Bremen, Germany
[2]University of Stuttgart, Germany

Abstract—Since its invention in the mid of eighties [1] Total Internal Reflection Microscopy (TIRM) has proven to be an effective technique to measure weak interactions between spherical colloidal particles and surfaces with a resolution of a few femtonewton. It is a single particle evanescent light scattering technique. In an experimental setup a laser beam is coupled into a prism and hits the glass-water interface with an angle slightly above the critical angle of total internal reflection. This generates an evanescent field near the interface that decays in the lower refractive index medium (water) with a characteristic penetration depth which depends on the angle of incidence. A colloidal particle that is dispersed in the medium will scatter light from the evanescent wave if it is in the vicinity of the surface. By registering a scattered intensity it is possible to deduce the particle-substrate distance. Compared to other methods for measure particle wall interactions like the surface force apparatus or the atomic force microscopy where a colloidal particle is attached to the tip, TIRM is the most sensitive technique because thermal fluctuations where limit the other methods in their resolution are exploited to determine the interaction potential. In this way forces in the order of a few femtonewton can be detected. TIRM has proven to be a valuable tool for the precise measurement of weak colloidal interactions as double layer forces, van der Waals forces, magnetic interactions and depletion forces. Review on TIRM can be found for example in [2, 3].

To compare experimental results with results of mathematical modeling an effective light scattering method is needed. For this purpose the Discrete Sources Method (DSM) has been chosen. The DSM is a well-known method for light scattering analysis, which has recently been applied for evanescent wave scattering [4].

1. Discrete Sources Method

For the theoretical modeling the Discrete Sources Method (DSM) has been chosen. The DSM is a well-known method for the analysis of light scattering. It has recently been applied to the evanescent wave scattering [4]. In frame of the DSM the mathematical statement can be presented as follows:

$$\begin{aligned} &\nabla \times \mathbf{H}_\zeta = jk\varepsilon_\zeta \mathbf{E}_\zeta; && \nabla \times \mathbf{E}_\zeta = -jk\mu_\zeta \mathbf{H}_\zeta && \text{in } D_\zeta, \quad \zeta = 0, 1, i, \\ &\mathbf{n} \times (\mathbf{E}_i - \mathbf{E}_0) = 0, && \mathbf{n} \times (\mathbf{H}_i - \mathbf{H}_0) = 0, && \text{at } \partial \mathrm{D} \\ &\mathbf{e}_z \times (\mathbf{E}_0 - \mathbf{E}_1) = 0, && \mathbf{e}_z \times (\mathbf{H}_0 - \mathbf{H}_1) = 0, && \text{at } \Sigma \end{aligned} \tag{1}$$

and radiation conditions at infinity.

Here, D_0 is an ambient media, D_1 is a glass prism, D_i is an interior particle domain ∂D is a particle boundary, Σ is a prism-air border, $\mathbf{n}$ is the outward unit normal vector to ∂D, $k = \omega/c$ and $\{\mathbf{E}_\zeta,\ \mathbf{H}_\zeta\}$ stands for the total field in the corresponding domainD_ζ. We assume that the exciting field $\{\mathbf{E}_1^i,\ \mathbf{H}_1^i\}$ is a plane wave propagating from D_1 at the angle θ_1 with respect to the z-axis and transmitting at the interface following Snell's law. Note that the total field in D_0 is a superposition of the refracted incident field $\{\mathbf{E}_0^i,\ \mathbf{H}_0^i\}$ and the scattered $\{\mathbf{E}_0^s,\ \mathbf{H}_0^s\}$ field. If Im $\varepsilon_\zeta, \mu_\zeta \leq 0$ (the time dependence for the fields is chosen as $\mathbf{exp}\{j\omega t\}$) and the particle surface is smooth enough $\partial D \subset C^{(1,\alpha)}$, then the above boundary-value problem is uniquely solvable.

We construct an approximate solution to the scattering problem (1) according to the DSM outlines [5]. The amplitudes of discrete sources are determined from the boundary conditions at the particle surface, which can be rewritten as

$$\mathbf{n} \times (\mathbf{E}_i - \mathbf{E}_0^s) = \mathbf{n} \times \mathbf{E}_0^i \qquad \mathbf{n} \times (\mathbf{H}_i - \mathbf{H}_0^s) = \mathbf{n} \times \mathbf{H}_0^i, \qquad \text{at } \partial D \tag{2}$$

To construct the fields of dipoles and multipoles analytically satisfying the transmission conditions at the plane interface Σ we apply the Green tensor for a stratified interface [6].

An approximate solution takes into account an axial symmetry of the particle and the polarization of an external excitation. For P-polarized excitation for fields presentations outside the particle the following electric

and magnetic vector potentials are used

$$\begin{aligned}
\mathbf{A}_{m,n}^{e,0} &= \{g_m^e(\eta,z_n)\cos(m+1)\phi; -g_m^e(\eta,z_n)\sin(m+1)\phi; -f_{m+1}(\eta,z_n)\cos(m+1)\phi\},\\
\mathbf{A}_{m,n}^{h,0} &= \{g_m^h(\eta,z_n)\sin(m+1)\phi; g_m^h(\eta,z_n)\cos(m+1)\phi; -f_{m+1}(\eta,z_n)\sin(m+1)\phi\},\\
\mathbf{A}_{0,n}^{e,h,0} &= \{0;\ 0;\ g_m^{h,e}(\eta,z_n)\}.
\end{aligned} \tag{3}$$

where $g_m^{e,h}$, f_m Fourier harmonics of the corresponding Green tensor components [4]. For the total field inside the particle we define the following vector potentials:

$$\begin{aligned}
\mathbf{A}_{\mathrm{m,n}}^{\mathrm{e,i}} &= \{\mathrm{J}_{\mathrm{m}}^{\mathrm{i}}(\eta,\mathrm{z_n})\cos(\mathrm{m}+1)\phi; -\mathrm{J}_{\mathrm{m}}^{\mathrm{i}}(\eta,\mathrm{z_n})\sin(\mathrm{m}+1)\phi; 0\},\\
\mathbf{A}_{m,n}^{h,i} &= \{J_m^i(\eta,z_n)\sin(m+1)\phi; J_m^i(\eta,z_n)\cos(m+1)\phi; 0\},\\
\mathbf{A}_{0,n}^{e,h,i} &= \{0;0;J_0^i(\eta,z_n)\}.
\end{aligned} \tag{4}$$

Here $J_m^i(\eta,z_n) = j_m(k_i,R_{\eta z_0})(\rho/R_{\eta z_0})^m$, $j_m(\cdot)$ is the cylindrical Hankel function, $\{z_n\}_{n=1}^{\infty}$ is a dense set of the points distributed over a segment $\Gamma_z^i \in D_i$ of the axis of symmetry. The approximate solution for the P-polarized excitation can be represented as

$$\begin{pmatrix} \mathbf{E}_\varsigma^n \\ \mathbf{H}_\varsigma^n \end{pmatrix} = \sum_{m=0}^{M}\sum_{n=1}^{N_\varsigma^m}\left\{ p_{mn}^\varsigma \mathbf{D}_1^\varsigma \mathbf{A}_{m,n}^{e,\varsigma} + q_{mn}^\varsigma \mathbf{D}_2^\varsigma \mathbf{A}_{m,n}^{h,\varsigma}\right\} + \sum_{n=1}^{N_\varsigma^0} r_n^\varsigma\ \mathbf{D}_1^\varsigma\ \mathbf{A}_{0,n}^{e,\varsigma}. \tag{5}$$

Where $\mathbf{D}_1^\varsigma = \left(\frac{j}{k\varepsilon_\varsigma\mu_\varsigma}\nabla\times\nabla\times,\ -\frac{1}{\mu_\varsigma}\nabla\times\right)^T$, $\mathbf{D}_2^\varsigma = \left(\frac{1}{\varepsilon_\varsigma}\nabla\times,\ \frac{j}{k\varepsilon_\varsigma\mu_\varsigma}\nabla\times\nabla\times\right)^T$.
The case of an S-polarized excitation can be considered in a similar way [4].

Now we would like briefly describe the numerical realization of the computational algorithm. As mentioned above representation (5) satisfies all the conditions of the scattering problem (1) except the transmission conditions at the particle surface (2). These conditions are used to determine the unknown amplitudes of discrete sources $\{p_{mn}^{0,i}, q_{mn}^{0,i}, r_n^{0,i}\}$. Since the scattering problem geometry is axially symmetric with respect to the Z-axis and discrete sources are distributed over the axis of symmetry, fulfilling the transmission conditions (2) at surface ∂D can be reduced to a sequential solution of the transmission problems for the Fourier harmonics of the fields. So, instead of matching the fields on the scattering surface, we can match their Fourier harmonics separately thus reducing the approximation problem on the surface to a set of problems enforced at the particle surface generatrix $\Im$. By solving these problems one can determine the discrete sources amplitudes $\{p_{mn}^{0,i}, q_{mn}^{0,i}, r_n^{0,i}\}$.

For the determination of amplitudes the generalized point-matching technique is used [7]. The DSM is a direct method and hence it allows to solve the scattering problem for the entire set of incident angles θ_1 and for both polarizations (P and S) at the same time. Besides, the numerical scheme provides an opportunity to control the convergence of the approximate solution to the exact one by a posterior error estimation [5].

After the amplitudes of the discrete sources (DS) are determined, the far field pattern $\mathbf{E}_\infty(\theta,\varphi)$ of the scattered field, can be calculated. It is determined at the upper part of the unit semi-sphere $\Omega = \{0^\circ \le \theta < 90^\circ,\ 0^\circ \le \phi \le 360^\circ\}$ and is given by

$$\mathbf{E}_0^s(\mathbf{r})/\mathbf{E}^0(0) = \frac{\exp\{jk_0r\}}{r}\mathbf{F}(\theta,\varphi) + O\left(r^{-2}\right) \quad r\to\infty$$

Using asymptotical estimation of the Weyl-Sommerfeld integrals of the Green's tensor components, the representation of the elements of a far field pattern gets a form of finite linear combinations of elementary functions [4]. This circumstance ensures an economical computer analysis of the scattering characteristics in the wave zone.

One of the most important scattering characteristics is an intensity of scattered light

$$I^{P,S}(\theta_0,\theta,\varphi) = \left|F_\theta^{P,S}(\theta_0,\theta,\varphi)\right|^2 + \left|F_\varphi^{P,S}(\theta_0,\theta,\varphi)\right|^2 \tag{6}$$

where $F_{\theta,\varphi}^{P,S}(\theta_0,\theta,\varphi)$ are the components of the far field pattern for P (5) and S polarized incident wave, in a spherical coordinate system θ, φ.
In the paper we will examine the objective response function, which presents the intensity scattered into a certain solid angle:

$$\sigma_s^{P,S}(\theta_0) = \int_\Omega I^{P,S}(\theta_0,\theta,\varphi)\ d\omega \tag{7}$$

where $\Omega = \left\{ 0 \le \varphi \le 360^0;\ 0;\ 0 \le \theta \le \theta_{NA} \right\}$, θ_{NA} is an angle, which corresponds to the Numerical Aperture (NA) of the objective lens in accordance with $\theta_{NA} = \arcsin(NA/n_0)$.

The number of matching points where the DS amplitudes are defined increases till the necessary accuracy of the results is achieved. The DS number usually is 2-3 times less then the number of the matching points on the particle generatrix. As a rule the discrete sources are deposited on the axis of symmetry inside the particle. The order of multipoles (M) is a priori defined from the condition that the plane wave approximation should be less then 0.1%. The detailed algorithm of matching point's choice and deposition is described in [6].

2. Results and Discussion

In the paper we would like to present some results of numerical modelling of the TIRM calibration curve. As an example we took a PSL sphere of diameter $D = 1.6\,\mu$m at wavelength of 658nm. In figures the objective response (7) is plotted as a function of particle–prism distance. To show the results we have chosen two incident angles which differ from critical one. In Figure one the results for PP, PS, SP and SS polarization are presented for deviation of the incident angle from critical one by 0.58°, and in figure 2 similar results are presented for deviation of 2.6°. In both figures the intensity for P polarized light has less distortions then for S polarized. It is in good agreement with a multiple reflections theory, as the reflectance for P-polarized light is always lower then for S-polarized one.

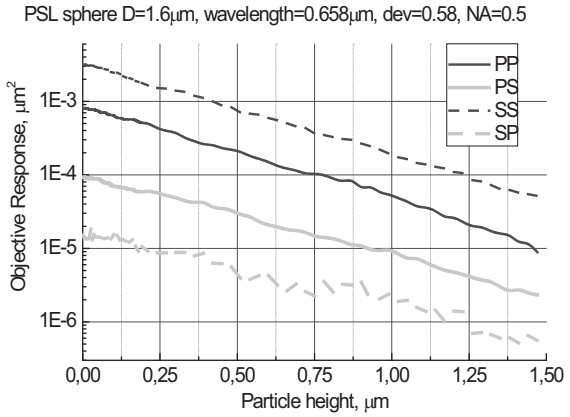

Figure 1: The objective response (7) versus particle-prism distance for a PSL sphere of diameter $D = 1.6\,\mu$m for different polarizations and incident angle deviation of 0.58°.

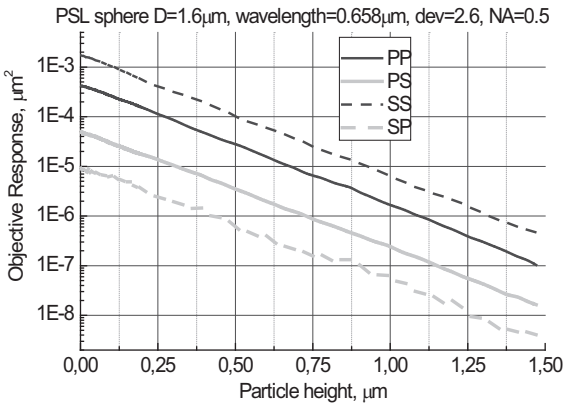

Figure 2: The objective response (7) versus particle-prism distance for a PSL sphere of diameter $D = 1.6\,\mu$m for different polarizations and incident angle deviation of 2.6°.

In the oral presentation more numerical results and their comparison with experimental data will be shown.

Acknowledgement

Authors would like to acknowledge financial support of this work by Deutsche Forschungsgemeinschaft (DFG).

REFERENCES

1. Prieve, D. C., F. Luo, and F. Lanni, *Faraday Discussions Chemical Society*, Vol. 83, 297, 1987.
2. Prieve, D. C., *Advances in Colloid and Interface Science*, Vol. 82, 93, 1999.
3. Bike, S. G., *Current Opinion in Colloid and Interface Science*, Vol. 5, 144, 2000.
4. Eremin, Y. and T. Wriedt, "Large dielectric particle in an evanescent wave field near a plane surface," *Opt. Comm.*, Vol. 214, 39, 2002.
5. Eremin, Y., *J. Commun. Technology and Electronics*, Vol. 45, 269, 2000.
6. Eremin, Y., N. Orlov, and A. Sveshnikov, *Generalized Multipole Techniques for Electromagnetic and Light Scattering*, Wriedt, T., Ed., Elsevier Science, Amsterdam, 39, 1999.
7. Voevodyn, V. and A. Kuznetsov, *Matrices and calculations. Science*, Moscow, 1982.

T-matrix Simulation of Plasmon Resonances of Particles on or Near a Surface

N. Riefler and T. Wriedt
University of Bremen, Germany

Abstract—We present the light scattering response of gold and silver particles on or near surfaces consisting of different materials. A comparison is made between a particle near a perfectly conducting surface and near a gold surface. The resulting scattering diagrams are found to be different. Beyond this, an approximation with a mirror particle shows little aggrement with a particle near a metal surface. Furthermore, we compare the spectral response of a combination of gold and silver materials for particles at different heights.

1. Introduction

Surface plasmons of small noble metal spheres can be detected as resonance peaks in the measured light scattering spectra. Transmission dark field microscopy is a technique where only the particles scatter light into the direction of the microscope objective. Such a measuring device can visualize very small particles as colored discs. The surface plasmon resonance frequency from a nonspherical particle or from a particle aggregate is different compared with a single spherical particle. With this effect, measuring techniques which use white light as illumination are capable to differ between aggregated particles and a single particle because of their different color. Even when a bio receptor molecule attached to a gold or silver sphere detects a biomolecular counterpart, the resonance frequency changes.

In the following we first describe the underlying scattering theory. Then we give some simulation examples of particles on or near a surface. We compare these results to some approximations found in the literature. This leads us to statements about the applicability of these approximations.

2. Theory

The scattering geometry is shown in Figure 1. The incident field $\vec{\mathbf{k}}_0$ and the particle are in the same medium.

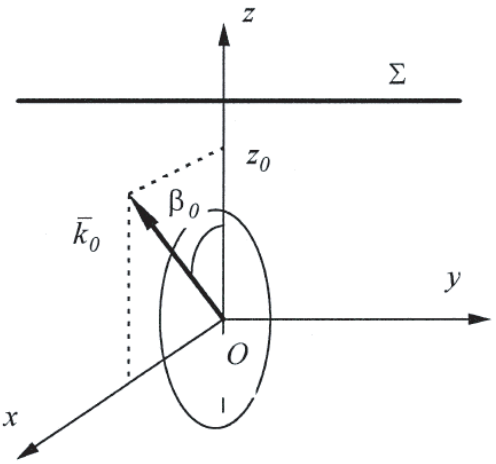

Figure 1: Scattering geometry; the z-axis is perpendicular onto Σ, the boundary surface.

In the T-matrix formalism using the null-filed method, the scattered intensities I_{sca} are calculated from the scattered field coefficients f_{mn} and g_{mn}. These coefficients are related to the T-matrix [1]:

$$\begin{bmatrix} f_{mn} \\ g_{mn} \end{bmatrix} = \mathbf{T} \left(\begin{bmatrix} a_{mn_1} \\ b_{mn_1} \end{bmatrix} + \begin{bmatrix} f^R_{mn_1} \\ g^r_{mn_1} \end{bmatrix} \right) \tag{1}$$

with the T-matrix $\mathbf{T} = T_{mn,mn_1}$ of the particle, the total incident field coefficients $a_{mn_1} = a^0_{mn_1} + a^R_{mn_1}$ and $b_{mn_1} = b^0_{mn_1} + b^R_{mn_1}$ consisting of the direct ($a^0_{mn_1}$ and $b^0_{mn_1}$) and the reflected ($a^R_{mn_1}$ and $b^R_{mn_1}$) incident fields,

and the coefficients $f^R_{mn_1}$ and $g^R_{mn_1}$ representing the fields scattered on the particle and reflected back from the surface to the particle. The $a^R_{mn_1}$ and $b^R_{mn_1}$ involves the Fresnel reflection coefficients. The scattered reflection coefficients for the interacting fields $f^R_{mn_1}$ and $g^R_{mn_1}$ are related to the scattered fields f_{mn_1} and g_{mn_1}:

$$\begin{bmatrix} f^R_{mn} \\ g^R_{mn} \end{bmatrix} = \mathbf{A} \begin{bmatrix} f_{mn} \\ g_{mn} \end{bmatrix}. \tag{2}$$

T is calculated from well known algorithms [2] and **A** can be found using radiating vector spherical wave functions [1]. By combining the matrix equations (2) and (3), the far field intensity can be computed. In the case of illumination from above ($\vec{\mathbf{k}}_0$ shows in the reversed direction) the incident field is calculated in the way described so far. If the incident angle β_0 get bigger than the critical angle $\theta_c = arcsin(n_1/n_2)$ with $n_1 < n_2$ and n_1 and n_2 are the refractive indicees of the medium above and below Σ, respectively, then the incident field from above will be totally reflected on Σ. However, an evanescent wave with typical exponential decrease is traveling into medium n_2. In this case the Fresnel transmission coefficients used in the T-matrix method are changing [3].

3. Results

We calculate intensities at different scattering angles over the visible spectrum of wavelengths of small particles with diameter $d = 80\,\text{nm}$. The intensities will be detector integrated over a range of $\theta_{NA} = 25°$ which corresponds to a numerical aperture of $NA = n\sin(\theta_{NA})$ of the objective lens. The particles consist of silver or gold. The wavelength dependend refractive indices are interpolated values from Johnson et al., [4]. The numerical aperture depends on the medium surrounding the particle. We use air, water and immersion oil with an assumed constant refractive index.

In Figures 2 and 3 the scattering diagrams of three systems are shown. In all systems the particle is a gold sphere and the scattering medium is air. The incident beam angle with respect to the normal is $\beta_0 = 30°$ with an incident wavelength of $\lambda = 570\,\text{nm}$. For that wavelength, the refractive index of the particle is $n = 0.296 + i2.899$. We first compare a system consisting of two spheres without an interface ('double-sphere' in the legend) with diameter $d = 80\,\text{nm}$ and distance $z = 4\,\text{nm}$. The idea behind this system can be found in electrostatic theory where a system consisting of two point charges shows an identical electrical field compared to a point charge near a conducting plane. We approximate this second system with a surface having a nearly perfect conducting material ('sphere-perfect-conductor' in the legend of the figures) with a wavelength independant refractive index $n = 0.00001 + i80$, and the distance between the surface of the sphere to the plane surface is half of the first system ($z = 2\,\text{nm}$). This idea is confirmed with Figure 2.

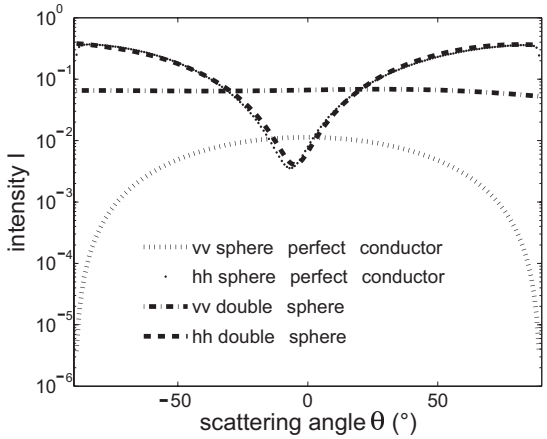

Figure 2: Scattering diagrams of a sphere before a perfectly conduction plane and two spheres.

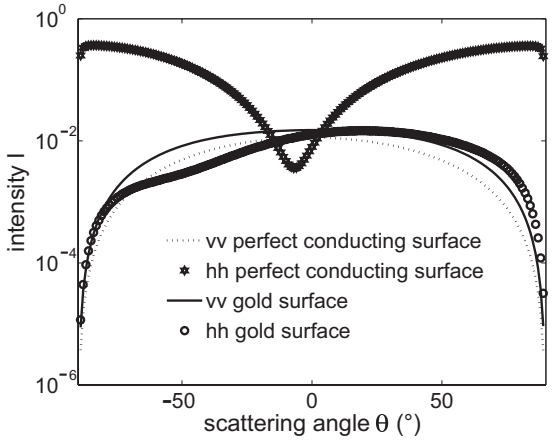

Figure 3: Scattering diagrams of a sphere before a perfectly conduction plane and before a gold surface.

Considering the different coordinate systems one can see that the horizontal-horizontal polarized scattering diagrams are very similar. The vertical-vertical polarized scattering diagram of the second system cannot be a straight line because of the Fresnel reflectance coefficients.

In contrast to the different geometries of the systems used in Figure 2, the two systems of Figure 3 are geometrically identical. A gold sphere with diameter of $d = 80\,\text{nm}$ is located near an infinite surface (distance between surface of the sphere to the plane surface $z = 2\,\text{nm}$). The only difference is that in the first system the surface is an approximation of a perfectly conducting material used above, while in the second system the plane surface consists of gold ('gold surface' in the legend). The first system with the perfectly conducting surface shows a distinct minimum. This is due to a very small transmission coefficient and a corresponding reflection coefficient of nearly $r = 1$ [3]. Therefore the particle near to the surface is excited 'ideally' from a plane wave. In the second system this minimum vanishes because the Fresnel transmission coefficient do not vanish and therefore the particle is excited differently.

We state that the scattering response of a particle located near a noble metal surface cannot be well approximated with a system consisting of two identical spheres because of the different Fresnel reflection coefficients.

Now we want to consider measurement problems where an optical device pick up the light spectrum scattered from an object on or near a surface. For example a gold particle within a liquid medium is illuminated from a wave at oblique incidence. For the following examples the bottom (substrate) is an optically thick layer. In practice this means a thickness of a few hundred nanometers of a noble metal [5]. The particle medium is water ($n = 1.333$). We first show the scattering diagram for a particle with diameter $d = 80\,\text{nm}$, $\beta_0 = 30°$ and $\lambda = 570\,\text{nm}$, but for three different heights (Figure 4). At a distance of $z = 200\,\text{nm}$, distinct minima appear because of multiple reflections between the particle (in the Rayleigh regime) and the surface. For a low distance these multiple reflections vanish and with it the minima.

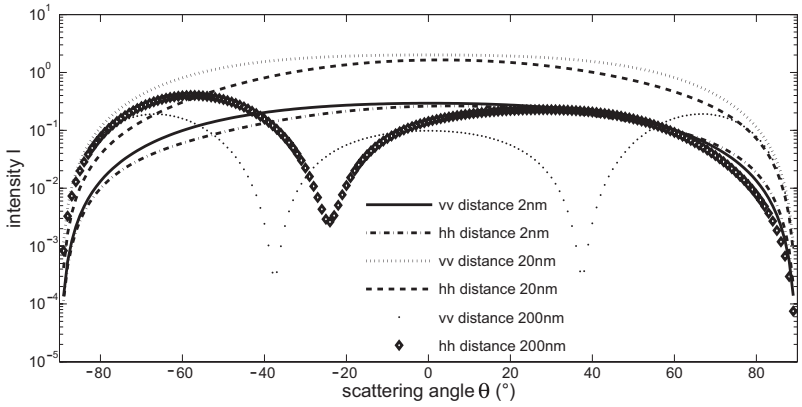

Figure 4: Comparison of the scattering diagram of three different systems.

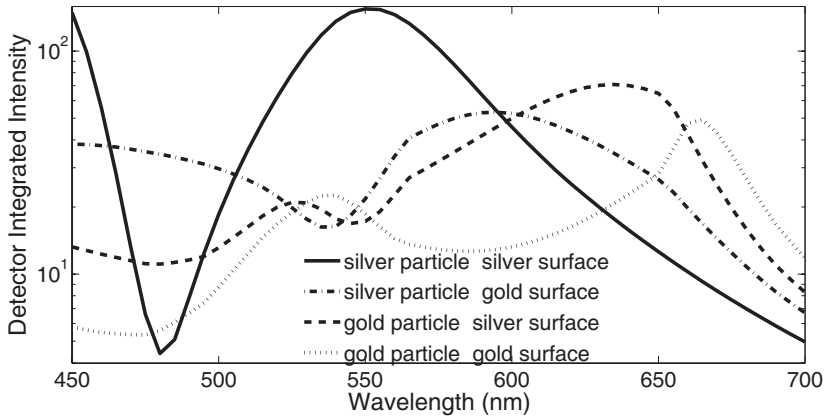

Figure 5: Detector integrated scattering diagrams of a particle at $z = 2\,\text{nm}$ in water.

In the following figures, the intensities are detector integrated values with an aperture angle of $\alpha = 25°$. The spectral resolution of the wavelengths is $\Delta\lambda = 5\,\text{nm}$. We use a spectrum of unpolarized incident waves ($\lambda = 450 \ldots 700\,\text{nm}$) which irradiates four different scattering systems:

- silver particle in water above a silver surface;
- silver particle in water above a gold surface;
- gold particle in water above a silver surface;
- gold particle in water above a gold surface.

For a distance between substrate surface and particle surface of $z = 2\,\text{nm}$ (this means a $z_0 = 42\,\text{nm}$ in Figure 1, the spectrum of detector integrated scattering intensities are shown in Figure 5. When the particle is situated higher at a distance of $z = 20\,\text{nm}$ above the noble metal surface ($z_0 = 60\,\text{nm}$), the resulting scattering response of the same four systems can be seen in Figure 6. A further increase of the height to $z = 200\,\text{nm}$ above the surface ($z_0 = 240\,\text{nm}$) results in Figure 7.

Last of all we want to compare the spectral scattering response for a gold particle near to a gold surface for three different media:

- gold particle in air ($n = 1.0$) above a gold surface;
- gold particle in water ($n = 1.333$) above a gold surface.
- gold particle in immersion oil ($n = 1.518$) above a gold surface.

We assume constant refractive index over all wavelengths of the media (air, water and oil). The spectral detector integrated intensities are shown in Figure 8.

The spectral response differs considerably. Especially the both liquid media show different characteristic spectras.

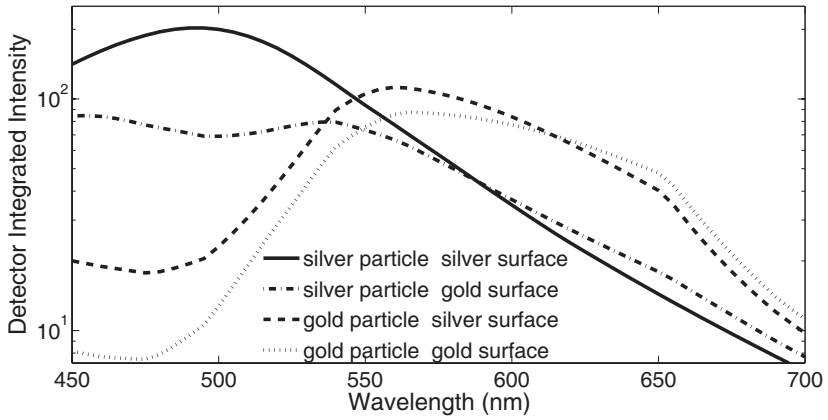

Figure 6: Detector integrated scattering diagrams of a particle at $z = 20\,\text{nm}$ in water.

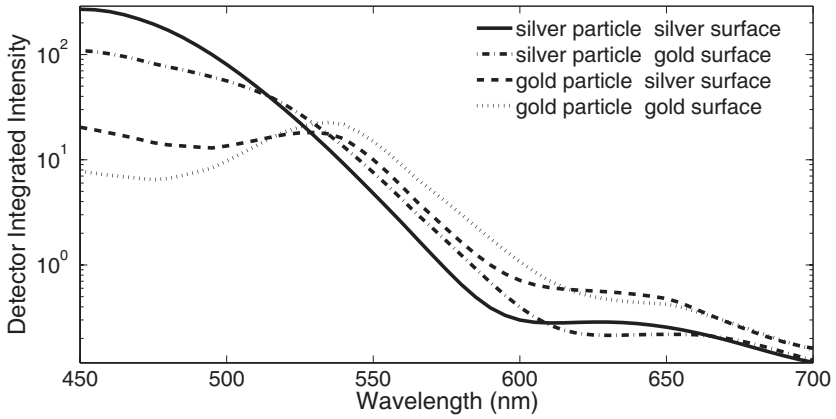

Figure 7: Detector integrated scattering diagrams of a particle at $z = 200\,\text{nm}$ in water.

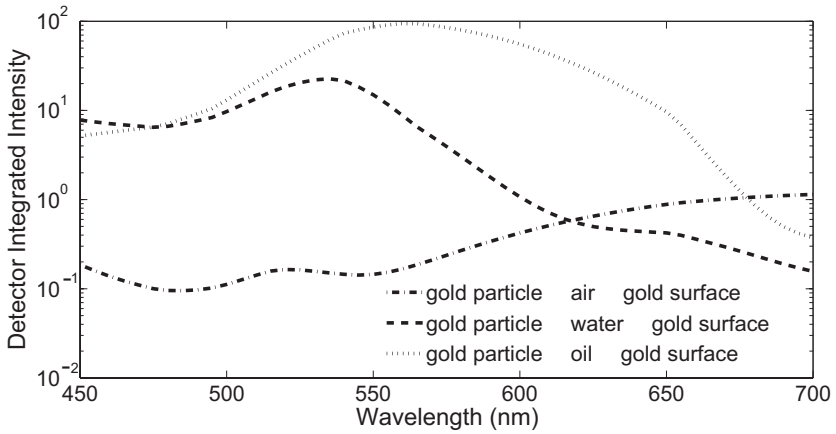

Figure 8: Spectrum of detector integrated intensities for different media (air, water and immersion oil); the particle position is $z = 200nm$.

4. Conclusion

We show that approximations like the double sphere system are far away from a qualitative similarity with the system under investigation. This means that simulations of the real circumstances are necessary, particulary if one needs quantitative statements of an observed system.

The results of the spectral simulations suggest that for increasing heights of a particle above the surface there is a shift of the intensity maximum towards lower wavelengths (see Figure 5–Figure 7). This fact may be used for measuring techniques. So altogehter, we want to emphasize the usage of exact techniques like the T-matrix method used for the simulations shown in this paper as a design tool for experimental investigations (e. g., [6]).

REFERENCES

1. Wriedt, T. and A. Doicu., "Light scattering from a particle on or near a surface," *Phys. Rev. B.*, Vol. 152, 376–384, 1998.
2. Doicu, A., Y. Eremin, and T. Wriedt, *Acoustic and Electromagnetic Scattering Analysis using Discrete Sources*, Academic Press, London, 2000.
3. Hecht, E., *Optics*, Addison Wesley, San Francisco, 2002.
4. Johnson, P. B. and R. W. Christy., "Optical constants of noble metals," *Phys. Rev. B*, Vol. 6, 4370–4379, 1972.
5. Born, M. and E. Wolf., *Principles of Optics.*, Pergamon Press, San Francisco, 1980.
6. Curry, A., G. Nusz, A. Chilkoti, and A. Wax, "Substrate effect on refractive index dependence of plasmon resonance for individual silver nanoparticles observed using darkfield microspectroscopy," *Opt. Expr.*, Vol. 13, 2668–2677, 2005.

Mean-field Theory of Light Scattering by Naturally Rough Surfaces

V. V. Lopushenko
Moscow State University, Russia

Scattering from rough surfaces is a subject of interest in many diverse research areas, such as optics, spectroscopy, remote sensing, sonar detection, radar imaging. The two classical and widely used methods to study scattering from two-dimensional rough surfaces are the Rayleigh or small-perturbation method (SPM) and the Kirchhoff or physical optics approxi-mation (KA) [1, 2]. The former is valid for small heights and slopes, and the latter is valid for high frequencies and large radii of curvature. In these regions of the surface parameters the two methods give useful results, but they do not overlap except those surfaces that have small and smooth roughness [3].

Therefore, strong interest persists to develop new analytical approaches to obtain better solu-tions in a domain where the accuracy of neither the KA nor the SPM is guaranteed. This makes alternative methods such as the mean-field theory (MFT) interesting since it may bridge the gap between the SPM and the KA. The MFT has been introduced quite recently [4, 5] and has not been systematically tested in the 2D case in scattering from substantially rough surfaces having root-mean square (RMS) height comparable with wavelength of the incident radiation. In this paper the MFT is applied to calculate incoherent scattering from 2D rough natural surfaces with power-law spectra, which are typical for fractal or ocean-like surfaces. An important fact to note is that the RMS/wavelength ratio is not assumed to be a small parameter, that is why both electric field and Green's tensor involved to the integral equation for scattered intensity are calculated numerically as solutions of the reference problem characterized by averaged refractive index.

To study a validity domain of the presented approach, some computer simulations have been made for the surfaces with ocean-like spectrum. The RMS heights of the considered surfaces were well beyond the usual SPM domain. The numerical comparison between the presented modification of the MFT and other approaches [3] show surprisingly good agreement in scattering diagrams plotted in the main incidence plane for both polarization cases.

REFERENCES

1. Beckmann, P. and A. Spizzichino, "The scattering of electromagnetic waves from rough surfaces," Macmillan, New York, 1963.
2. Voronovich, A. G., "Wave scattering from rough surface," 2nd edn, Springer, Berlin, 1998.
3. Soriano, G., C. A. Gu'erin, and M. Saillard, "Scattering by two-dimensional rough surfaces: comparison between the method of moments, Kirchhoff and small-slope approximations," *Waves Random Media*, Vol. 12, 63–83, 2002.
4. Sentenac, A. and J. J. Greffet., "Mean-field theory of light scattering by one-dimensional rough surfaces," *J. Opt. Soc. Am. A*, Vol. 15, No. 2, 528–532, 1998.
5. Lopushenko, V. V., "Calculation of Scattering from Microroughness of Filmed Wafers," *Proc. of the 4st Conference on Electromagnetic and Light Scattering by Nonspherical Particals: Theory and Applications*, 231–238, Vigo, Spain, September 20–21, 1999.

Rigorous Model for Gold Nanorods Spectra Examination Based on Discrete Sources Method

Y. A. Eremin
Moscow Lomonosov State University, Russia

Gold nanorods have received much attention in recent years due to their special electronic and optical properties. For example, the sensitivity of the plasmon resonance frequency toward the refractive index of the surroundings makes them suitable candidates for biological sensing applications [1]. For these applications gold nanorods of diameter from 15 nm up to 90 nm and having a variety of aspect ratios (length/diameter) from 2 to 12 are usually employed. They demonstrate an existence of several resonance peaks in the field of evanescent waves. The necessity to predict the positions and value of the frequency resonances requires to built computer model enables to perform a rigorous analysis of the scattering spectra. A lot of efforts have been spent developing rigorous models to examine light scattering from a nanorod deposited in a vicinity of a plane interface. Nevertheless the most approaches used so far do not account completely the interaction between field scattered by nanorod and the interface surface.

The model used here is based on asymmetrical version of the Discrete Sources Method (DSM) [2]. This technique constructs the scattered field everywhere outside a local obstacle as a finite linear combination of the fields resulting from electric dipoles distributed over an auxiliary surface located inside the obstacle. The Green Tensor of a half-space is incorporated to fit the transmission conditions enforced at the plane interface. Then the scattered field analytically satisfies transmission conditions at the interface, thus accounting for all interactions between particle and interface automatically. Internal field is represented on the basis of regular functions, which fit Maxwell's equations. So, the DSM solution constructed satisfies Maxwell's equations everywhere outside medium discontinuities, required infinity conditions and transmission conditions at the plane interface. Then the unknown DS sources amplitudes are to be determined from boundary conditions enforced at the surface of the local obstacle only.

It has been found that more stable results can be obtained by using pseudo-solution of an over-determined system of linear equations obtained by following the generalised point-matching technique. Select a set of matching points on the particle homogeneously covering the surface. Then distribute homogeneously DS over the auxiliary surface. In each DS point we choose three independent electric dipoles, which originate the scattered field. Then the linear system to be used for determining of the DS amplitudes is derived from matching the boundary conditions at the set of matching points. This procedure leads to an over-determined matrix and the DS amplitudes are evaluated by a pseudo-inversion technique [3]. The numerical scheme allows to consider all incidences and both polarization P and S at once. DSM computer model controls convergence and stability of the result obtained by a posterior evaluation of the surface residual. In the presentation computer simulating results associated with an influence of nanorod aspect ratio, orientation and exciting field polarization on the scattering spectra will be presented.

*Author would like to acknowledge support of this work by ADE Corporation, Westwood, MA, USA and Russian Foundation for Basic Research.

REFERENCES

1. Zhu, J., et al., "Shape dependent resonance light scattering properties of gold nanorods," *Materials Science and Engineering B*, Vol. 121, 199–203, 2005.
2. Eremin, Y. A., J. C. Stover, and N. V. Grishina, "Discrete sources method for light scattering analysis from 3D asymmetrical features on a substrate," *J. Quant. Spectrosc. Radiat. Transfer.*, Vol. 70, 421–431, 2001.
3. Grishina, N. V., Y. A. Eremin, and A. G. Sveshnikov, "Analysis of evanescent waves transformation based on Discrete Sources Method," *J. Commun. Techn. Electron.*, Vol. 49, 117–124, 2004.

Local Biosensor Operation Analysis Based on Discrete Sources Method Model

N. V. Grishina and Y. A. Eremin
Moscow Lomonosov State University, Russia

Interest in electromagnetic wave scattering by nanoshells has increased rapidly within the past years. Nanoshells represent a new type of nanoparticles composed of a dielectric core coated with a thin noble metallic shell. Such particles are of great interest in different applications due to their scattering behavior and ability to demonstrate plasmon resonance response in the visible range of optical spectrum. It has been found that the resonance frequency of a nanoshell depends on its properties: material, size, shape, shell thickness and etc. Varying those parameters enables to shift the resonance peak to a required frequency domain, in particular to the "transparent window" for biological tissue. Nanoshells used for biomedical applications are often called local biosensors [1]. The principle of a local biosensor operation is based on the evanescent waves transformation near water-glass interface. The light scattered by nanoshell is detected by objective lens. Even a small changing of the refractive index in the vicinity of the particle, caused by presence of irrelevant substances, leads to a shift of the resonance peak position. So, from detection of its position one can get information about refractive index of an ambient media in the vicinity of the sensor and detect its deviation from the known refractive index of ambient water [1].

During the last years a lot of effort has been spent developing rigorous model to predict light scattering from nanoshell deposited near a plane interface. Nevertheless the most approaches used so far do not account completely the interaction between nanoshell and interface. The model presented here is based on the Discrete Sources Method (DSM) [2, 3]. This technique constructs the scattered field everywhere outside an axial-symmetric layered particle as a finite linear combination of the fields resulting from multipoles distributed over the axis of symmetry inside the particle. The Green Tensor of a layered substrate is employed to account for the complete interaction of the particle with a stratified interface analytically [2]. The solution for the scattered field satisfies Maxwell's equations and required conditions at infinity. Then the unknown discrete sources amplitudes are determined from transmission conditions enforced at the layers of the particle [3].

DSM numerical scheme is based on axial symmetry of the scattering geometry (particle-interface). Exciting evanescent wave impinging the particle from prism surface is resolve in Fourier series with respect to the azimuth angle. This leads to the reducing surface approximation to a set of one dimensional approximating problems enforced at the layers profiles. To fit the transmission conditions we use generalized point-matching technique. Multipoles amplitudes are determined as pseudo-solutions over-determined systems of the linear equations. The DSM scheme enables to consider all incident angles and both polarization P and S at once. The DSM computer model controls convergence and stability of the results by a posterior evaluation of the surface residual at the particle layers. In the presentation computer simulating results relating to the biosensor synthesis, operation and sensitivity to a local changing of environment will be presented.

*Authors would like to acknowledge support of this work by ADE Corporation, Westwood, MA, USA and Russian Foundation for Basic Research.

REFERENCES

1. Raschke, G., et al., "Gold nanoshells improve single nanoparticles molecular sensors," *Nanoletters*, Vol. 4, 1853–1857, 2004.
2. Grishina, N. V., Y .A. Eremin, and A. G. Sveshnikov, "Analysis of evanescent waves transformation based on discrete sources method," *J. Commun. Techn. Electron.*, Vol. 49, 117–124, 2004.
3. Grishina, N. V., Y. A. Eremin, and A. G. Sveshnikov, "Analysis of the scattering properties of oxide particles at a layered substrate," *Physics Bulletin*, Vol. 54, No. 2, Moscow University, 2000.

Magnetic Nanostructure Hysteresis Loop Calculation for Modified Thin Film Multi-layer by Ion Irradiation

D. Bajalan
Vienna University of Technology, Austria

Abstract—The nonlinear dependence of magnetization on direction of the applied magnetic field and history is described by statistical domain behavior using phenomenological adaptive parameters (like: g [1], h [A/m], k [J/m^3], and q that are related to anisotropy, saturation field, static hysteresis loss, and pinning site density). The loop simulation data could be used also as parameters for thermal stability equation to calculate the relaxation time of the stored information on any magnetic nano particles (dots) of patterned magnetic media.

1. Introduction

Magnetic nanostructures are subjects of growing interest because of their potential applications in high density magnetic recording media and their original magnetic properties [1]. Multilayer thin films (like Co/Pt) are well known for their high magnetic anisotropy, and the origin of this high magnetic anisotropy has been the subject of interest for many researchers [2]. Demands for the continuous increase in the data storage density bring the challenge to overcome physical limits for currently used magnetic recording media [3]. Patterned magnetic media could be a way of realizing ultra high density storage media. Recently, demonstrations of areal recording density over 60 Gb/in^2 in both longitudinal and perpendicular magnetic recordings have been successfully made [4]. Determining the properties of small magnetic structures is extremely important for the development of data storage devices [5]. Better understanding of the micromagnetic processes in magnetic recording media is essential for developing novel materials for future ultrahigh density recording [6]. Good understanding of the noise mechanism in magnetic recording is required for developing heads and media for future applications [7].

In perpendicular recording, the magnetization pattern corresponding to the bits is provided perpendicular to the plane of the medium. The information is being stored in vertical domains or other structures of uniform magnetization [8]. The magnetic properties of an ultra thin multilayer can be patterned by controlled ion beam irradiation [9]. The basic step in this technique is to control the changes in the magnetic properties induced by the irradiation process.

In magnetic materials two characteristic length scales have to be considered [10]:

- at the atomic level, nearest neighbour exchange interaction is dominating,
- at a mesoscopic level, the domain wall width is the characteristic length dominating the magnetization reversal.

When the physical dimensions of a system become comparable to the interatomic spacing, strong modifications of the intrinsic magnetic properties (ordering temperature, magnetic anisotropy, spontaneous magnetization) are expected.

Micromagnetic modeling of the behavior of a nanostructured film beautifully describes the magnetization process, but requires a high calculational effort and long computation times. Furthermore, it is difficult to predict changes of the macroscopic physical behaviour due to variation of parameters. Phenomenological models, on the other hand, are very useful to simulate the behaviour of the magnetic material under the influence of varying parameters, especially when the parameters are based on physical constants.

2. Experiments

An assembly of ferromagnetic amorphous nanoparticles has been prepared by heavy ions irradiation of paramagnetic YCo_2 thin films [11, 12]. Several irradiation experiments carried out on YCo_2 samples have shown that fluences on the order 10^{12} U ions/cm^2 causes changes in magnetic properties of the samples [12]. Important changes are reported to take place after the irradiation:

- change of spontaneous magnetization, coercivity and initial susceptibility [12], and
- a distinct change of the anisotropy perpendicular to the film plane [11].

3. Energetic Model

The magnetic behaviour of magnetic moments is mainly described by the well known equations of Schrödinger (exchange interaction) and Landau, Lifshitz, and Gilbert (dynamics of magnetization reversal). Above this fundament is the shell of the physical constants describing spontaneous magnetization, anisotropy, magnetostriction, etc. The energetic model (EM) is designed as an interface between this shell and the macroscopic hysteresis phenomenon, able to predict many magnetic properties due to the relation of the parameters with the physical constants. The EM has been applied for different magnetization processes and materials [13–17].

The hysteresis of the magnetization M depending on the applied field H is described by the following equations, with the spontaneous magnetization M_s, the geometrical demagnetizing factor N_d, and the following phenomenological parameters:

1. g [1] related to anisotropy, reversible processes;
2. h [A/m] related to saturation field H_s, reversible processes;
3. k [J/m^3] related to static hysteresis loss, irreversible processes;
4. q [1] related to pinning site density, irreversible processes.

In the cases of large domains, the microscopic constant c_r describes the influence of reversal speed. The $\mathrm{sgn}(x)$ function provides the correct four quadrant calculation (with the related magnetization $m = M/M_s$):

$$H = H_d + \mathrm{sgn}(m)H_R + \mathrm{sgn}(m - m_o)H_I\,. \tag{1}$$

The first term of Eq. (1) describes linear material behaviour, using the demagnetizing field

$$H_d = -N_d M_s m\,, \tag{2}$$

the second term represents non-linear behaviour using the reversible field

$$H_R = h\Big[\big((1+m)^{1+m}(1-m)^{1-m}\big)^{g/2} - 1\Big]\,, \tag{3}$$

including saturation at a field $H_s(M_s)$, and the third term describes hysteresis effects like initial susceptibility χ_0, remanence M_r, coercivity H_c, static losses, and accomodation, using the irreversible field

$$H_I = \left(\frac{k}{\mu_0 M_s} + c_r H_R\right)\left[1 - \kappa \exp\Big(-\frac{q}{\kappa}|m - m_o|\Big)\right]. \tag{4}$$

For the initial magnetization, beginning with $M = 0$, $H = 0$, we set $m_o = 0$ and $\kappa = 1$. The function κ describes the influence of the total magnetic state at points of magnetization reversal. Therefore, κ (previous value κ_o) depends on the unit magnetization reversals $s = |m - m_o|$ up to this point of field reversal (m_o is the starting value of m at the last field reversal) with the simplification $e^{-q} \ll 1$:

$$\kappa = 2 - \kappa_o \exp\left[-\frac{q}{\kappa_o}|m - m_o|\right]. \tag{5}$$

The calculation always starts with the initial magnetization curve and m is increased stepwise (the stepwidth determines the desired resolution of the calculation), which gives the corresponding field by Eq. (1). At a point of field reversal κ is calculated by Eq. (5) and m_o is set to the actual value of m at this point. Then m is decreased stepwise until the next reversal point, etc.

3.1. Identification

The identification of the EM with measurements or data sheets can be done easily. At given M_s and N_d the parameters are directly calculated from special points of the hysteresis loop. Considering reference conditions, the index 0 is to indicate that the identification is done at a temperature $T = T_0$ without applied mechanical stress σ, using the following equations:

$$k_0 = \mu_0 M_s H_c \tag{6}$$

$$q_0 = \frac{M_s}{H_c}\frac{1 - N_d\chi_0}{\chi_0} \tag{7}$$

If χ_0 is not available one can also use the total static losses $w_l = \displaystyle\int_{-M_s}^{+M_s} H\mathrm{d}M + \int_{+M_s}^{-M_s} H\mathrm{d}M$ corresponding to the area of the closed major loop (upper and lower branch of hysteresis)

$$w_l = 4k\left(1 - \frac{2}{q}\right) \tag{8}$$

and we can write the equation for q_0 as

$$q_0 = \frac{8\mu_0 M_s H_c}{4\mu_0 M_s H_c - w_l}\,. \tag{9}$$

These relations allow even an estimation of M_s (at $c_r \approx 0$), using Eqs. (6), (7), and (9) to

$$M_s = \frac{2\chi_0 H_c}{1 - N_d\chi_0} + \frac{w_l}{4\mu_0 H_c}\,. \tag{10}$$

Furthermore, q_0 can also be determined by the reduced remanence m_r of the upper branch of a loop with the measured reduced maximum magnetization m_m. Using f_q as a factor related to m_r,

$$f_q = \left[(1+m_r)^{1+m_r}(1-M_r)^{1-m_r}\right]^{g_0/2} - 1\,, \tag{11}$$

we identify q_0 as

$$q_0 = \frac{2}{m_m - m_r}\ln\frac{2H_c}{H_c - h_0 f_q + N_d M_s m_r} \tag{12}$$

By using f_g as a factor related to m_g which is the reduced magnetization at $H = H_g$, in the knee of the lower branch of the hysteresis,

$$f_g = \frac{1}{\ln\sqrt{(1+m_g)^{1+m_g}(1-m_g)^{1-m_g}} - \ln 2}\,, \tag{13}$$

hence g_0 is

$$g_0 = f_g \ln\frac{H_g - H_c - N_d M_s m_g}{H_s - H_c - N_d M_s} \tag{14}$$

Using f_c as a factor related to m_r and m_m,

$$f_c = 1 - 2\exp\left[q_0\frac{m_r - m_m}{2}\right], \tag{15}$$

the microscopic constant describing the domain (grain) geometry ratio becomes

$$c_r = \frac{f_q\frac{H_s - H_c - N_d M_s}{M_s}\exp g_0 \ln 2 - f_c\frac{H_c}{M_s} + N_d m_r}{\left(f_q\frac{H_s - H_c - N_d M_s}{M_s}\exp g_0 \ln 2 + f_c\frac{H_c}{M_s}\right) - N_d m_r} \tag{16}$$

Finally, the identification equation of h_0 is

$$h_0 = \frac{H_s - H_c - N_d M_s}{(c_r + 1)(\exp[g_0 \ln 2] - 1)} \tag{17}$$

If H_s is not available, one can estimate H_s from the measured maximum field H_m at m_m using the approximation $H_s \gg H_c + N_d M_s$. Using f_h as a factor related to m_g and m_m

$$f_h = \frac{\ln\sqrt{(1+m_m)^{1+m_m}(1-m_m)^{1-m_m}} - \ln 2}{\ln\sqrt{\frac{(1+m_g)^{1+m_g}(1-m_g)^{1-m_g}}{(1+m_m)^{1+m_m}(1-m_m)^{1-m_m}}}} \tag{18}$$

we find

$$H_s = (H_m - H_c - N_d M_s m_m)\left(\frac{H_m - H_c - N_d M_s m_m}{H_g - H_c - N_d M_s m_g}\right)^{f_h}\,. \tag{19}$$

If N_d of the experimental arrangement is unknown then it can be estimated roughly by the differential susceptibility χ_c at coercivity of a measured hysteresis loop:

$$N_d \approx \left.\frac{1}{\chi_c}\right|_{H=H_c}\,. \tag{20}$$

If N_d of the sample is rather large so that the magnetization curve is strongly sheared ($M_r N_d > H_c$), then it can be necessary to identify g_0 and c_r by the backsheared curve ($N_d = 0$).

3.2. Calculation

The calculations have been done as following: At a given $N_d = 0.47$, the parameters $g_0 = 5.24$, $h_0 = 2.79\,\mathrm{kA/m}$, $k_0 = 1.10\,\mathrm{kJ/m^3}$, and $q_0 = 8.79$ are identified for the perpendicular hysteresis at $\Phi = 5{\cdot}10^{12}\,\mathrm{ions/cm^2}$ with $M_s = 20\,\mathrm{kA/m}$. In the next step we vary only M_s in order to calculate the hysteresis of the other irradiation cases. Using Eqs. (6) and (7), we find the dependencies

$$H_c = \frac{k_0}{\mu_0 M_s} \tag{21}$$

and

$$\chi_0 = \frac{\mu_0 M_s^2}{k_0 q_0 + \mu_0 M_s^2 N_d} \tag{22}$$

which strongly affects the shape of the hysteresis Curve.

4. Conclusions

The rapid development of magnetic recording leads to a large increase of the bit density. Multilayer thin films with a perpendicular magnetic anisotropy devices may play an active role in the development and establishment of future storage technologies. Patterning magnetic media is a potential solution for ultrahigh density magnetic recording [18]. Ion beam modification of magnetic layers may be the possible future of ultra high density magnetic recording media.

After ion irradiation of YCo_2 thin films with different fluence values, the measured magnetizazion curves clearly show a perpendicular aniyotropy [11]. The shape of the hysteresis loops depends strongly on M_s, which is predicted by the EM. It turns out that H_c is inversely proportional to M_s and χ_0 is proportional to M_s^2, if N_d is neglected. As the EM parameters are also related to anisotropy it will be possible also to calculate the direction dependence of these magnetization curves, which is subject to further work.

REFERENCES

1. Jamet, M., W. Wernsdorfer, C. Thirion, D. Mailly, V. Dupuis, P. Mélinon, and A. Pérez, *Phys. Rev. Lett.*, Vol. 86, 4676, 2001.
2. Yamada, Y., T. Suzuki, H. Kanazawa, and J. C. Osterman, *J. Appl. Phys.*, Vol. 85, 5094, 1999.
3. Lapicki, A., K. Kang, and T. Suzuki, *IEEE Trans. Magn.*, Vol. 38, 2589, 2002.
4. Papusoi, C. and T. Suzuki, *J. Magn. Magn. Mater.*, Vol. 240, 568, 2002.
5. Kirk, K. J., J. N. Chapman, and C. D. W. Wilkinson, *J. Appl. Phys.*, Vol. 85, 5237, 1999.
6. Kisker, H., N. Abarra, Y. Yamada, P. Glijer, and T. Suzuki, *J. Appl. Phys.*, Vol. 81, 3937, 1997.
7. Phillips, G. N., T. Suzuki, K. Takano, and M. Takahashi, *J. Magn. Magn. Mater.*, Vol. 193, 434, 1999.
8. Suzuki, T., *Magneto-Optic Recording Thin Films, in: I. M. H. Francombe (Ed.), Handbook of Thin Film Devices Magnetic, Vol. 4, Magnetic Thin Film Devices*, Academic Press, 2000.
9. Ferre, J., C. Chappert, H. Bernas, J.-P. Jamet, P. Meyer, O. Kaitasov, S. Lemerle, V. Mathet, F. Rousseaux, and H. Launois, *J. Magn. Magn. Mater.*, Vol. 198, 191, 1999.
10. Noziéres, J. P., M. Ghidini, N. M. Dempsey, B. Gervais, D. Givord, G. Suran, and J. M. D. Coey, *Nucl. Instr. and Meth. in Phys. Res. B*, Vol. 146, 250–259, 1998.
11. Givord, D., J. P. Noziéres, M. Ghidini, B. Gervais, and Y. Otani, *J. Magn. Magn. Mater.*, Vol. 148, 253–259, 1995.
12. Solzi, M., M. Ghidini, and G. Asti, *Magnetic Nanostructures*, Vol. 4, 123, 2002.
13. Hauser, H. and P. L. Fulmek, *J. Magn. Magn. Mater.*, Vol. 133, 32, 1994.
14. Fulmek, P. L. and H. Hauser, *J. Magn. Magn. Mater.*, Vol. 157, 361, 1996.
15. Hauser, H. and R. Grössinger, *J. Appl. Phys.*, Vol. 85, 5133, 1999.
16. Andrei, P., L. Stoleriu, and H. Hauser, *J. Appl. Phys.*, Vol. 87, 6555, 2000.
17. Grössinger, R., H. Hauser, M. Dahlgren, and J. Fidler, *Physica B*, Vol. 275, 248, 2000.
18. Devolder, T., C. Chappert, Y. Chen, E. Cambril, H. Launois, H. Bernas, J. Ferre, and J. P. Jamet, *J. Vac. Sci. Technol. B*, Vol. 17, 3177, 1999.

Energetical Model Interpretation of Thermal Stability by Changing Direction of the Magnetization of Nano Magnetic Structure

D. Bajalan
Vienna University of Technology, Austria

Abstract—The nonlinear dependence of magnetization on the direction of the applied magnetic field and history is described by statistical domain behavior using phenomenological adaptive parameters (like: g[1], $h[A/m]$, $k[J/m^3]$, and q that are related to anisotropy, saturation field, static hysteresis loss, and pinning site density). The loop simulation data could be used also as parameters for thermal stability equation to calculate the relaxation time of the stored information on any magnetic nano particles (dots) of patterned magnetic media.

1. Introduction

Magnetic nano particle thermal stability calculation is essential for development of patterned ultra high magnetic storage media. The use of reliable model (like: Energetic Model (EM) in the predication of non linear ferromagnetic materials properties [1], wich may depend also on direction and history of magnetization) is very important. EM simulation of hysteresis opens a very big opportunities to calculate values of parameters which we then use directly for interpretation of the stability condition of stored information on a nano magnetic structure. The main idea behind that is to change the direction of the applied field H and then see the stability conditions on a given nano bit volume. The value of the f_{BS} depends strongly on K_u and the volume of the nano structure which holds the stored magnetic information (a what so-called nano bit or nano dot). Research and development teams in companies implementing nano-technology are gaining more and more importance in the field of sensor systems and material science.

2. Interpretation of Magntization Processes and Result

The EM calculates the magnetic state of ferromagnetic materials by minimizing the total energy density w_T [1] (see Table 1) as the sum of the energy density:

Table 1: Relation between k_u, and relaxation time τ at dot-width $D_w = 22\,\text{nm}$ and $T = 10\,\text{K}$, as a result of dependence of magnetization on direction of the applied magnetic field at different Φ with values($0°$, $45°$, $90°$), where f_{BS} condition is satisfied.

magnetization direction Φ	k_u [J/m^3]	τ [Years]
$90°$	602.51	22.3×10^3
$45°$	1110.67	22.5×10^{15}
$0°$	1895.46	12.4×10^{35}

$$w_T = w_H + w_M \tag{1}$$

Where:

$$w_H = -\mu_0 \vec{M} \cdot \vec{H} \tag{2}$$

of the applied field $\vec{H}$ and the magnetization $\vec{M}$ and the material energy density

$$w_M = w_d + w_R + w_I \tag{3}$$

The latter term is divided into the energy density of demagnetizing fields w_d and into contributions described by statistical domain behaviour: The reversible energy density w_R and the irreversible energy density w_I. It's very important to verify the components of the demagnetization factor that appears with in the magnetization process of a nano magnetic particles. Magnetization hysteresis loops, which display the magnetic response of

a magnetic sample to an external field, have been widely used to characterize the behavior of nanostructured magnetic materials [2]. The effective demagnetization factor (or total-demagnetziation factor) is compound of two types (where Nd is a geometric and Ni is the inner demagnetizing factor, e. g., due to the magnetostatic stray Fields within the microstructure of grains or particles) as the following:

$$N_e = N_d + N_i \tag{4}$$

The characteristic features of the hysteresis loop are dependent on the material, the size and shape of the entity, the microstructure, the orientation of the applied magnetic field with respect to the sample, the magnetization history of the sample, and the demagnetization factor.

3. Equations

If N_d of the experimental arrangement is unknown then it can be estimated roughly by the differential susceptibility χ_c at coercivity of a measured hysteresis loop [3]:

$$N_d \approx \frac{1}{\chi_c}\Big|_{H=H_c} \tag{5}$$

The relation between N_d, $N_{e,0}$, $N_{e,\pi/2}$, and K_u is given as

$$N_d = N_{e,0} - \frac{K_0}{K_u}(N_{e,\pi/2-N_{e,0}}) \tag{6}$$

$$K_u = \frac{K_0}{N_{e,0} - N_d}(N_{e,\pi/2-N_{e,0}}) \tag{7}$$

K_u which is important for calculation of the bit stability factor (see Table 1) is also related to the N_d that depends on the magnetization. Further the identification of K_0 is given by

$$K_0 = \mu_0 M_s^2 \tag{8}$$

4. Conclusion

Nano-technology is providing a critical bridge between the physical sciences and engineering, on the one hand, and modern molecular biology on the other. Materials scientists, for example, are learning the principles of the nanoscale world by studying the behavior of biomolecules and biomolecular assemblies. Nano-technology will increase its influence in electrical engineering and electrical materials strongly. The need for further development in nano-technology is required. Companies with market-oriented innovation, research and advanced development strategies like EVGroup have had important positions and an excellent reputation in the practical implementation of nano-technology. New and light magnetic devices will be invented to make life in the 21st century more functional and the researchers have to gain more knowledge of quantum effects within nano-meter body size. The energetic model is used to identify hysteresis by changing the the direction of the applied field to nano magnetic particles of irradiated samples. Effects of changing the direction of the magnetization field on thermal stability and relaxation time could be then calculated. Choosing a reliable model (EM) for hysteresis simulation of nano magnetic particles is essential. Demands for the continuous increase in the data storage density bring the challenge to overcome physical limits for currently used magnetic recording media [5–14].

Acknowledgement

I would like to express my words of gratitude to EV Group for their support.

REFERENCES

1. Hauser, H., *J. Appl. Phys.*, Vol. 96, 2753, 2004.
2. Sun, L., Y. Hao, C.-L. Chien, and P. C. Searson, *IBM J. Res. Develop.*, Vol. 49, 79, 2005.
3. Bajalan, D., H. Hauser, and P. L. Fulmek, *Physica B*, Vol. 343, 384, 2004.
4. Bajalan, D., H. Hauser, and P. L. Fulmek, *Progress in Electromagnetic Research Symposium (March 28 to 31), 2004*, Pisa, Italy, Extended paper (ISBN 88 8492 268 2), 456, 2004.
5. Solzi, M., M. Ghidini, and G. Asti, *Magnetic Nanostructures*, Vol. 4, 123, 2002.

6. Lapicki, A., K. Kang, and T. Suzuki, *IEEE Trans. Magn.*, Vol. 38, 589, 2002.
7. Sellmyer, D. J., C. P. Luo, and Y. Qiang, *Handbook of Thin Film Devices Magnetic, Nanomaterials and Magnetic Thin Films*, Academic Press, Vol. 5, 337, 2000.
8. Laughlin, D. E. and B. Lu, Seagate Research Center, Materials Science and Engineering Department and Data Storage Systems Center, Carnegie Mellon University, Pittsburgh, 2, 2001.
9. Binns, C. and M. J. Maher, *New Journal of Physics*, Vol. 4, 85.1, 2002.
10. MacMathuna, D., Surface studies of nanomagnetic systems, A thesis submitted to the University of Dublin, Trinity College, Physics Department, 2002.
11. Speliotis, D. E., Presented at the THIC Meeting at the Naval Surface Warfare Cente Center Carderock Bethesda, Digital Measurement Systems/ADE Technologies, 4, 2000.
12. McHenry, M. E., M. A. Willard, and D. E. Laughlin, *Progress in Materials Science*, Vol. 44, 291, 1999.
13. Jamet, M., W. Wernsdorfer, C. Thirion, D. Mailly, V. Dupuis, P. Mélinon, and A. Pérez, *Phys. Rev. Lett.*, Vol. 86, 4676, 2001.
14. Bajalan, D., H. Hauser, and P. L. Fulmek, *4th Int. Symposium on HMM*, University of Salamanca, Vol. 8, 78, 2003.

Innovation Use of Nano Technology in Magnetic Storage Devices and Nano Computers

D. Bajalan
Vienna University of Technology, Austria

J. A. Aziz
University Sains, Malaysia

Abstract—The fluence of ion irradiation on polycrystalline thin films affects both anisotropy and spontaneous magnetisation M_s. The dependence of coercivity and initial susceptibility on M_s is predicted by a hysteresis model considering the balance of energy with good qualitative agreement.

1. Introduction

Demands for the continuous increase in the data storage density bring the challenge to overcome physical limits for currently used magnetic recording media [1, 2]. Ferromagnetic nano-particles of different polycrystalline thin films have been formed by heavy or light ion irradiation [2–4]. Although this modification technique may be a way to produce nano-magnetic particles, there are some critical size limits of nanomagnetic structures like the superparamagnetic limit (SPML) which faces magnetic nanotechnology. The magnetic properties of thin films are strongly influenced by their structure [5]. Small changes in the way a thin film is produced often give rise to large changes in some of the magnetic properties of the thin film [6]. This is best understood by observing how the microstructure of the film changes with processing and then correlating the microstructure directly with the properties of the thin film [6]. The behaviour of magnetic nanoparticles has fascinated materials scientists for decades [7]. Magnetic nanostructures have become a centre of great interest in the scientific community and in industry as the core technologies behind magnetic recording devices [8]. And the magnetic properties of an ultra thin multilayer can be patterned by controlled ion beam irradiation [4]. There are fundamental limits due to the atomic nature of matter which may impose ultimate physical bounds to nanofabrication and miniaturization [9]. Over the past several decades, amorphous and more recently nano-crystalline materials have been investigated for applications in magnetic devices [10]. The benefit found in the nanocrystalline alloys stem from their chemical and structural variations on a nano-scale which are important for optimizing magnetic recording devices [10].

2. Irradiation Process and Results

Several irradiation experiments carried out on the Co/Pt multi-layers samples (A1, A2, and A3 see Table 1) cause changes in the magnetic properties of the thin films [1, 4]. High aspect ratio silica masks on Co/Pt multi-layers were obtained by e-beam lithography and reactive ion etching with feature sizes down to 30 nm for lines and 20 nm for dots [3]. He+ ion irradiation of the magnetic layers through these masks was used to pattern the magnetic properties [3] (with fluences between 2.10^{14} and 2.10^{16} ions/cm^2 [4]). After mask removal, high resolution and high density, planar magnetic nano-structures were obtained [3]. The results of the irradiation show perfectly square hysteresis loops at room temperature, the coercive field decreasing progressively to zero [4]. The high perpendicular anisotropy of Pt/Co multi-layers originates from the interfaces between the layers [11]. Other experminents carried out on YCo_2 samples (thin polycrystalline film targets of polycrystalline with thicknesses of approximately 1 μm [[12]) have shown that fluences in range of 10^{12} U ions/cm^2 cause changes in magnetic properties of the samples [1]. The result of these experiments were changes of the anisotropy perpendicular to the film plane [1], and change of spontaneous magnetisation, coercivity and initial susceptibility [13].

2.1. Equations and Calculation

The energetic model (EM) [14] is used to calculate the dependence of the shape of the hysteresis loop on M_s. The parameters of the model are calculated directly from measurements of special points of the hysteresis loop. The identification of the parameters is done at reference conditions (index 0) at a temperature $T = T_0$ without any applied mechanical stress σ, and at given M_s and N_e (N_e is the effective demagnetizing factor which is the sum of the geometric demagnetizing factor N_d and the inner demagnetizing factor N_i). The following equations show how to determine the parameter of the model from spontaneous magnetization M_s, coercivity H_c, and

from the effective demagnetization factor N_e.

$$k_0 = \frac{\mu_0 M_s H_c}{1 - 2\exp(-q_0)} \tag{1}$$

k in J/m^3 related to static hysteresis loss (irreversible processes), and

$$q_0 = \frac{\mu_0 M_s^2}{k_0} \frac{1 - N_e \chi_0}{\chi_0} \tag{2}$$

q (dimensionless) is related to pinning site density (irreversible processes). Using Eqs. (1) and (2) with the approximation $\exp[-q_0] \ll 1$, we find the dependencies

$$H_c = \frac{k_0}{\mu_0 M_s} \tag{3}$$

and

$$\chi_0 = \frac{\mu_0 M_s^2}{k_0 q_0 + \mu_0 M_s^2 N_e} \tag{4}$$

which strongly affects the shape of the hysteresis. Figure 1 shows the initial magnetization curves calculated and measured major hysteresis loops in dependence of the measured value of M_s. No other change of the parameter values has been made. Table 1 shows the result of the evaluation of the equations above. Figure 2 shows the initial magnetization curves calculated with the parameters depending on M_s due to irradiation, compared to measurements.

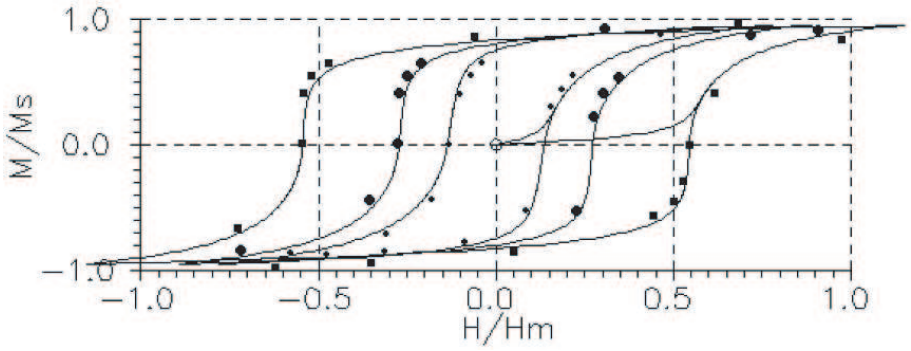

Figure 1: Calculated hysteresis loops for thin Films after different ion irradiation fluences perpendicular to the film plane and measured points. The H-values are related to the maximum field $H_m = 160\,\mathrm{kA/m}$. The Mvalues are related to the respective saturation values of $\mathrm{M}_s = 20\,\mathrm{kA/m}$, $\mathrm{M}_s = 40\,\mathrm{kA/m}$, and $M_s = 60\,\mathrm{kA/m}$ 1. Only these values have been changed to calculate the different major hysteresis loops.

3. Anisotropy Energy after Irradiation

The anisotropy energy k_u is essential for evaluation of the thermal stability condition on a given bit. For the three irradiated samples (A1, A2, A3), k_u was calculated (Eq. 5).

$$k_u = \frac{H_k \mu_0 M_s}{2} \tag{5}$$

4. Nano Bits Stability Factor and Its Relaxation Time Calculation

Assuming a factor f_{BS} a simple abbreviation for "bit stability factor", which represents the information stability of stored data on a given nano-bit, where: $f_{BS} = k_u V_{nano}/k_B T$, V_{nano} is the nano magnetic structure volume, $k_u V_{nano}$ is the energy barrier (ΔE), and $k_B = 1.38 \times 10^{-23}$ J/deg Boltzmann constant. The magnetic stored information on a nano dot is then stable: if only the condition ($f_{BS} > 40$) is satisfied [16]. The relaxation time (time duration of stored information) or switching time of stored information τ can be obtained from the Arrhenius relation as:

$$\tau = \frac{1}{f_0} \exp(f_{BS}) \tag{6}$$

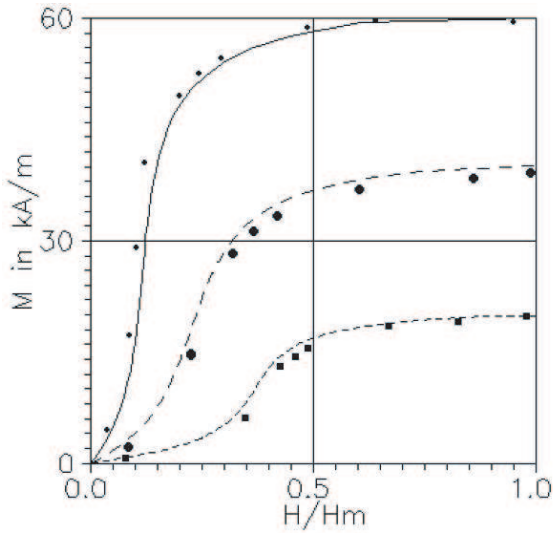

Figure 2: Calculated initial hysteresis curves loops for thin films after different ion irradiation fluences perpendicular (Tab. 1) to the film plane and measured points. The H-values are related to the maximum field $H_m = 160\,\mathrm{kA/m}$. The calculation has been done by varying the value of M_s, only.

Table 1: Macroscopic hysteresis features depending on M_s [14].

Φ	[ions/cm^2]	A1, 10^{12}	A2, $5 \cdot 10^{12}$	A3, $2 \cdot 10^{13}$
M_s	[kA/m]	20	40	60
χ_0	[1]	0.157	0.199	0.536
H_c	[kA/m]	43.6	21.8	14.5

Where f_0 is the thermal attempt frequency [17], which is usually assumed to be $10^9\ s^{-1}$. The irradiation of the samples (A1, A2, A3) with different fluences as shown in Table 1, caused changes of the calculated values of k_u for each sample. Hence different values of f_{BS} and τ were calculated (see Table 2).

Table 2: Relation between k_u, and relaxation time τ at dot-width $D_w = 22\,\mathrm{nm}$ and T=10 K, as a result of irradiation, where f_{BS} condition is satisfied.

samples	k_u [J/m^3]	τ [Years]
A_1	592.51	20.3×10^2
A_2	1017.67	23.6×10^{16}
A_3	1975.46	11.8×10^{38}

5. Conclusion

Magnetic nano-structures are subject of growing interest because of their potential applications in high density magnetic recording media and their original magnetic properties [11, 14–16]. The rapid development of magnetic recording leads to a large increase of the bit density. Multilayer thin films with perpendicular magnetic anisotropy devices may play an active role in the development and establishment of future storage technologies. Patterning magnetic media is a potential solution for ultrahigh density magnetic recording [3]. The shape of hysteresis loops depends strongly on M_s, where H_c is inversely proportional to M_s, and χ_0 is proportional to M_s^2. Thermal stability is one of the serious issues for developing high density recording, and thus much effort has been made to overcome this issue [18]. The idea to use a regular array of physically isolated grains/dots

promises an improvement in thermal stability of the recorded bits [19]. The anisotropy energy k_u is essential for evaluation of the thermal stability condition on a given bit, because k_u value is used in calculation of bit stability factor f_{BS}. A given nano bit is then thermaly stable: if only the condition ($f_{BS} > 40$) is satisfied.

Acknowledgement

I would like to express my words of gratitude to Prof. H. Hauser, TU-WIEN.

REFERENCES

1. Solzi, M., M. Ghidini, and G. Asti, *Magnetic Nanostructures*, Vol. 4, 123, 2002.
2. Lapicki, A., K. Kang, and T. Suzuki, *IEEE Trans. Magn.*, Vol. 38, 589, 2002.
3. Devolder, T., C. Chappert, Y. Chen, E. Cambril, H. Launois, H. Bernas, J. Ferre, and J. P. Jamet, *J. Vac. Sci. Technol. B*, Vol. 17, 3177, 1999.
4. Ferre, J., C. Chappert, H. Bernas, J.-P. Jamet, P. Meyer, O. Kaitasov, S. Lemerle, V. Mathet, F. Rousseaux, and H. Launois, *J. Magn. Magn. Mater.*, Vol. 198, 191, 1999.
5. Sellmyer, D. J., C. P. Luo, and Y. Qiang, "Handbook of thin film devices magnetic, nanomaterials and magnetic thin films," *Academic Press*, Vol. 5, 337, 2000.
6. Laughlin, D. E. and B. Lu, Seagate Research Center, Materials Science and Engineering Department and Data Storage Systems Center, Carnegie Mellon University, Pittsburgh, 2, 2001.
7. Binns, C. and M. J. Maher, *New Journal of Physics*, Vol. 4, 85.1, 2002.
8. MacMathuna, D., "Surface studies of nanomagnetic systems," A thesis submitted to the University of Dublin, Trinity College,Physics Department, 3, 2002.
9. Speliotis, D. E., Presented at the THIC Meeting at the Naval Surface Warfare Cente Center Carderock Bethesda, "Digital measurement systems/ADE technologies," 4, 2000.
10. McHenry, M. E., M. A. Willard, and D. E. Laughlin, *Progress in Materials Science*, Vol. 44, 291, 1999.
11. Jamet, M., W. Wernsdorfer, C. Thirion, D. Mailly, V. Dupuis, P. Mélinon, and A. Pérez, *Phys. Rev. Lett.*, Vol. 86, 4676, 2001.
12. Noziéres, J. P., M. Ghidini, N. M. Dempsey, B. Gervais, D. Givord, G. Suran, and J. M. D. Coey, *Nucl. Instr. and Meth. in Phys. Res. B*, Vol. 146, 250, 1998.
13. Givord, D., J. P. Noziéres, M. Ghidini, B. Gervais, and Y. Otani, *J. Magn. Magn. Mater.*, Vol. 148, 253, 1995.
14. Bajalan, D., H. Hauser, and P. L. Fulmek, *Physica B*, Vol. 343, 384, 2004.
15. Bajalan, D., H. Hauser, and P. L. Fulmek, *4th Int. Symposium on HMM*, Vol. 8, 78, University of Salamanca, 2003.
16. Hauser, H., D. Bajalan, and P. L. Fulmek, *Progress in Electromagnetic Research Symposium (March 28 to 31), 2004*, Pisa, Italy, Extended paper (ISBN 88 8492 268 2), 667, 2004.
17. Sun, L., Y. Hao, C.-L. Chien, and P. C. Searson, *IBM J. Res. Develop.*, Vol. 49, 79, 2005.
18. Mochidaa, M. and T. Suzuki, *J. Appl. Phys.*, Vol. 10, 8644, 2002.
19. Lapicki, A., K. Kang, and T. Suzuki, *IEEE Trans. Magn.*, Vol. 38, 2589, 2002.

Thin Nanoporous Films with a Honeycomb Structure: Internal Fields, Spectral and Scattering Properties

A. N. Ponyavina and R. A. Dynich
National Academy of Sciences of Belarus, Belarus

N. V. Gaponenko and G. K. Malyarevich
Belarusian State University of Informatics and Radioelectronics, Belarus

Nanoporous thin films with a honeycomb structure fabricated at aluminum electrochemical anodization are now of a great interest because of their unique ability to light spectral and angular selection [1, 2]. Utilizing a self-organized matrix of porous anodic alumina (PAA) is considered to be very promising for applications in microelectronics, magnetic recording, formation of nanotubes, etc. [3]. An attractive optical application of the PAA is connected with imbedding of the luminescent centers, for example ions or semiconductor nanocrystalls [4]. Strong transformation of luminescence spectra and angular distribution of light passed through the PAA are due to multiple scattering, local field enhancements into pores and density of states effects caused by a 2 D photon-crystal structure of the PAA.

New opportunities for these effects controlling may arise when pores are infiltrated with colloidal solutions of noble metallic nanoparticles (MNP). The related joint photonic–electronic confinement becomes possible to manifest at the spectral range of the MNP surface plasmon resonances. In order to determine the most favorable conditions we have developed a calculation method and made numerical simulations of internal fields, spectral and scattering properties in dependence on the PAA and MNP structural parameters.

The PAA films were considered as a high-ordered array of finite circular cylinders, parallel to each other and oriented perpendicularly to a planar substrate. Previously [1] we have developed a model of light propagation through the correlated cylinders ensemble that based on the statistical theory of multiple wave scattering considering single cylinder scattering with the use of the volume integral equation formalism [5]. Now we propose the modification of this scheme applied to the PAA infiltrated with colloidal solutions of the MNP.

Using this approach we have analyzed the PAA transmission spectra and field distribution into the pores at different pore sizes and materials embedded under condition of incident light directed along a pore axis. We have found a strong shift of the PAA transmission spectra short-wavelength cut-off boundary with a pore size enlarging. Theoretical results have shown a good agreement with experimental data. We have also established a possibility to increase the steepness of the cut-off boundary and to create a band type of the PAA transmission spectra by the MNP embedding. The transmission spectra modification is found to be accompanied by strong changing of the local internal field picture and scattering properties.

*The work was supported by the International Scientific Technical Center, Grant #B-276-2.

REFERENCES

1. Vereshchagin, V. G., R. A. Dynich, and A. N. Ponyavina, *Opt. Spectrosc.*, Vol. 87, 116–121, 1999.
2. Lutich, A. A. and I. S. Molchan, *Physics, Chemistry and Application of Nanostructure (Nanomeeting-2003)*, Editors Borisenko, V. E., S. V. Gaponenko, and V. S. Gurin, 256–259, 2003.
3. Thompson, G. E. and G. C. Wood, *Nature*, Vol. 290, 231, 1981.
4. Gaponenko, N. V., I. S. Molchan, A. A. Lutich, and S. V. Gaponenko, *Solid State Phen*, Vol. 97–98, 251–258, 2004.
5. Goodman J. J., B. T. Draine, and P. J. Flatau, *Opt.Letters.*, Vol. 16, 1198–1200, 1991.

Fast Computation of Diffraction by Finite-size Multilayered Arrays of Cylinders

Y.-J. Zhang and E.-P. Li
Institute of High Performance Computing, Singapore

Scattering by gratings or arrays of cylinders has been extensively studied for many years in the areas of remote sensing and optics. Scattering matrix method (SMM), also called T-matrix method, is the most popular method used for the calculation of multiple scattering among all the cylinders. SMM utilizes the T-matrix to describe the scattering property of each single cylinder and the addition theorems of cylindrical harmonics to take account of mutual couplings. So it is viewed as a kind of semianalytical method. Recently, many authors found new applications of scattering matrix method on the simulation of finite size photonic crystal devices. Scattering matrix method is much faster than those purely numerical methods such as finite difference time domain (FDTD) or finite element method (FEM). However, its computational complexity is still $O(N^2)$. This prohibits its further applications in large size devices, where N stands for the total harmonics numbers used to expand the fields for all cylinders.

In this paper, a novel algorithm, named as fast multipole accelerated scattering matrix method (FMA-SMM), is proposed to speed up the solution of SMM. Fast matrix method (FMM) has already been used to solve the integral equations of 2D scattering problems. The principal formula is the integration expression of zero-order Hankel function over the range of polar angle. It can be named as the fast multipole expression of zero-order Hankel function. Since Higher order, instead of only zero-order, Hankel functions are often involved in SMM, FMM could not be used directly. Fortunately, we derived the general fast multipole expressions for any order Hankel functions by using the lowering and rising operators of cylindrical harmonics. Through numerical investigations, we found that the higher order Hankel functions requires larger group size to reach specific error criterion. This has not been pointed out before since only zero-order Hankel function was investigated in previous publications. This new finding is especially important in successful implementation of the algorithm. The general expressions derived convert the dense coupling matrix in SMM into the combination of sparse matrices, namely aggregation matrix, translation matrix and disaggregation matrix. Thus results in a lower computational complexity of $O(N^{1.5})$ when iterative method is used to solve the final equations. The details of implementation will be presented to guarantee the accuracy of the algorithm. The accuracy and efficiency of FMA-SMM are verified by several numerical examples. A large array with more than 2,000 dielectric rods is analyzed to show the advantage of this novel fast algorithm.

A Numerical Method for the Analysis of Electromagnetic Scattering by Three Dimensional Magnetodielectric Body

A. G. Dmitrenko and T. N. Pastuhova
Tomsk State University, Russia

It is of considerable interest for researchers to study scattering of radio waves by a homogeneous 3 D magnetodielectric body. This interest arises from the need to solve a number of important problems in radar, meteorology, biology and atmospherical optic (see for example [1]).

Today, the different methods for the analysis of considered problem are existing. These methods base on differential forms of Maxwell's equations or integral relations of electromagnetic theory. But computer codes realized these methods are extraordinary in expenses of computer resources, especially for nonaxisymmetric scatterers.

In the last years, the method of discrete sources named in West as generalized multipole technique was applied to solving problems of electromagnetic wave scattering by bodies of different physical nature [2]. In particular, in [2] (Chapter 8) the version of discrete sources method for analysis of electromagnetic scattering by arbitrary shaped magnetodielectric body was proposed. In this version a system of discrete sources in the form of pair electric dipoles was used. These dipoles were located inside and outside magnetodielectric body on auxiliary surfaces homothetic to the surface of the body and oriented tangentially to them.

In the planning report the generalized variant of [2] will be proposed. The generalization consist of addition pair tangentially oriented magnetic dipoles in each point of electric dipoles location. The mathematical formulation of the variant and briefly description of capabilities of the developed software package will be done. The advantages of using of combined (electric and magnetic dipoles) system of discrete sources will be discussed. Some results illustrated the influence of nonaxisymmetry of body on bistatic cross section will be reported.

REFERENCES

1. Havemann, S. and A. J. Baran, *J. Quant. Spectrosc. Radiat. Transfer*, Vol. 70, 139, 2001.
2. *Generalized Multipole Techniques for Electromagnetic and Light Scattering* (Ed. by T. Wriedt), Amsterdam, Elsevier Science, 1999.

Rough Surface Characterization by Profilometer at Spatial Frequencies Appropriate for Light Scattering Predictions

J. C. Stover
The Scatter Works, Inc., USA

A study has been underway to provide a better scattering model for front surface reflectors that are optically rough. Scatter from optically smooth surfaces (mirrors) is well related to surface roughness by using Rayleigh-Rice vector perturbation theory. This expression relates the bidirectional reflectance distribution function (BRDF) to the surface power spectral density (PSD) for given set of scattering parameters (incident angle, wavelength and polarization). There is a one to one relationship and either quantity can be found if the other is measured. Thus for optically smooth surfaces the perturbation relationship could be checked by changing the scattering parameters. This resulted in different BRDF expressions, but for smooth, clean front surface reflectors the same PSD was found. Unfortunately the situation is not so easy for optically rough surfaces.

Since the one to one relationship between BRDF and PSD no longer exists for rough surfaces several different PSDs can produce the same BRDF. This makes calculation of the PSD from the BRDF impossible, and it becomes necessary to characterize the surface PSD with a profilometer. This raises a couple of problems. First, profilometers report 1-D PSDs. That is, they consider spatial frequencies propagating only in the direction of the scan, but BRDF is related to 2-D PSDs, which contain frequencies propagating on the surface in all directions. Secondly, most profilometers have a high frequency cutoff of about $0.1\,\mu\mathrm{m}^{-1}$. For visible light this corresponds to light scattered into a three degree cone about the specular beam. The rest of the scattering hemisphere cannot be predicted from profilometer generated PSDs, and thus these PSDs cannot be used to check the rough surface scattering model.

This presentation discusses the issues associated with solving these two problems. The 1-D to 2-D problem is solved by working with isotropic surfaces where a conversion expression can be used. The high frequency cutoff issue is more difficult. To solve this, a correction transfer function has to be found for the profilometer. This is developed by measuring a 2-D optically smooth surface and relating the profilometer PSD to that found using the perturbation expression. This is then applied to the measured PSDs of the rougher surfaces. A serious concern is the assumption of linearity (in profilometer response) that may not be true for the rougher surfaces; however, at least early modeling results seem close enough that this may not be an issue.

Of equal importance to the rough surface scattering modeling that this work will facilitate is the issue of specifying optics for low scatter with profilometer measurements. Although used throughout the optics industry, it is simply an indicator — not metrology.

Extended Discrete Sources Method Model for Extremal Scatterers

D. E. Sukhanov
Moscow Lomonosov State University, Russia

Light scattering analysis used in nanotechnology and biophotonics has been a subject of interest in last decades. This is primarily due to the variety of practical applications it is encountered in, for example, aerosol analysis, investigation of air pollution, radio wave propagation in the presence of atmospheric hydrometers, weather radar problems, analysis of contaminating particles on the surface of silicon wafers, remote sensing, etc. Special attention has been paid to extremely shaped particle light scattering problems. Methods being implemented to solve such problems are usually expensive in computer resources, especially if the size of the scattering object relative to the wavelength of the incident radiation is big. Another problem arises if scattering body is asymmetrical. In this case one has to implement more sophisticated methods than he might have been able to use in case of axis-symmetrical obstacle. So advanced methods are constantly developed to solve these both problems mentioned above. We introduce here a new approach which allows one to reach these goals.

Light scattering by extremely shaped local obstacle is considered here. The model used here is based on symmetrical version of the Discrete Sources Method (DSM) [1]. This technique constructs the scattered field everywhere outside a local obstacle as a finite linear combination of the fields resulting from electric and magnetic multipoles distributed over an auxiliary segment of the obstacle's axis of revolution inside the obstacle. Then the scattered field analytically satisfies transmission conditions at the obstacle's surface. Internal field is represented on the basis of regular functions, which fit Maxwell's equations [2]. So, the DSM solution constructed satisfies Maxwell's equations everywhere outside the obstacle, required infinity conditions and transmission conditions at the obstacle's surface. Then the unknown DS sources amplitudes are to be determined from boundary conditions enforced at the surface of the local obstacle.

It has been found that more stable results can be obtained by using pseudo-solution of an over-determined system of linear equations obtained by following the generalised point-matching technique. Select a set of matching points on the particle homogeneously covering the surface. Then distribute homogeneously DS over the auxiliary segment of scatterer's axis of revolution. In each DS point we choose three independent electric multipoles and three independent magnetic mutipoles, which originate the scattered field. Then the linear system to be used for determining of the DS amplitudes is derived from matching the boundary conditions at the set of matching points. This procedure leads to an over-determined matrix and the DS amplitudes are evaluated by a pseudo-inversion technique [3]. The numerical scheme allows one to consider all incidences and both polarization P and S at once. DSM computer model controls convergence and stability of the result obtained by a posterior evaluation of the surface residual. In the presentation computer simulating results associated with an influence of obstacle's aspect ratio, orientation and exciting field polarization on the scattering spectra will be presented.

*Authors would like to acknowledge support of this work by the Russian Foundation for Basic Research.

REFERENCES

1. Eremin, Y. and A. G. Sveshnikov, "Discrete sources method in electromagnetic scattering problems," *Electromagnetics*, Vol. 13, 1–22, 1993.
2. Eremin, Y., "Complete system of functions for the study of boundary value problems in mathematical physics," *Sov. Phys. Dokl.*, Vol. 32, No. 8, 635–637, 1987.
3. Doicu, A., Y. Eremin, and T. Wriedt, "Acoustic and electromagnetic scattering analysis using discrete sources," Academic Press, New York, 2000.